Effect of annealing on the electrical resistivity of Kondo lattice $CeRh_2Ga_2$

Physica Scripta

PAPER

Effect of annealing on the electrical resistivity of Kondo lattice $CeRh_2Ga_2$

V K Anand[1,2,3,*], **D T Adroja**[4,5], **Aarti**[3], **A Bhattacharyya**[6] and **B Lake**[1]

[1] Helmholtz-Zentrum Berlin für Materialien und Energie GmbH, Hahn-Meitner Platz 1, D-14109 Berlin, Germany
[2] Department of Mathematics and Physics, University of Stavanger, 4036 Stavanger, Norway
[3] Department of Physics, University of Petroleum and Energy Studies, Dehradun, Uttarakhand, 248007, India
[4] ISIS Facility, Rutherford Appleton Laboratory, Chilton, Didcot, Oxon, OX11 0QX, United Kingdom
[5] Highly Correlated Matter Research Group, Physics Department, University of Johannesburg, PO Box 524, Auckland Park 2006, South Africa
[6] Department of Physics, Ramakrishna Mission Vivekananda Educational and Research Institute, Belur Math, Howrah 711202, West Bengal, India
[*] Author to whom any correspondence should be addressed.

E-mail: vivekkranand@gmail.com **and** devashibhai.adroja@stfc.ac.uk

Keywords: Kondo semimetal, heavy fermion, electrical resistivity, fermi-liquid

OPEN ACCESS

RECEIVED
27 October 2023

REVISED
2 April 2024

ACCEPTED FOR PUBLICATION
12 April 2024

PUBLISHED
25 April 2024

Abstract

$CeRh_2Ga_2$, which crystallizes in $CaBe_2Ge_2$-type primitive tetragonal structure (space group $P4/nmm$), is known to exhibit Kondo lattice heavy fermion behavior and is proposed to be a potential candidate for Weyl-Kondo semimetal phase. Here we examine the effect of annealing, particularly on the electrical resistivity of polycrystalline $CeRh_2Ga_2$. A comparative study of the powder x-ray diffraction (XRD), magnetic susceptibility $\chi(T)$, heat capacity $C_p(T)$ and electrical resistivity $\rho(T)$ data of both as-arc-melted and annealed $CeRh_2Ga_2$ samples are presented. The XRD patterns of both as-arc-melted and annealed samples look similar. No marked effect of annealing could be clearly seen in the temperature dependences of χ and C_p data. However, the effect of annealing is clearly manifested in the T dependence of ρ, particularly at low temperatures. At low-T the $\rho(T)$ data of as-arc-melted $CeRh_2Ga_2$ follow a T^2 temperature dependence (Fermi-liquid feature), whereas the $\rho(T)$ data of annealed $CeRh_2Ga_2$ exhibit an upturn (semimetal-like feature).

1. Introduction

Ce-based compounds are well known to present diverse electronic properties such as unconventional superconductivity, Kondo insulator/semimetal, quantum criticality, heavy fermion and non-Fermi liquid behavior etc. The electronic ground state of Ce-compounds are determined by the strength of the hybridization between the conduction and f-electrons and strongly competing RKKY (Ruderman-Kittel-Kasuya-Yosida), Kondo and crystal electric field (CEF) interactions [1–7]. Among these the compounds belonging to the 122 series CeT_2X_2 (T=transition element, X = Ge, Si) have attracted considerable research interests within the condensed matter community by presenting many interesting properties. The majority of the CeT_2X_2 compounds form either in $ThCr_2Si_2$-type body-centered tetragonal (bct) structure (space group $I4/mmm$) or in $CaBe_2Ge_2$-type primitive tetragonal structure (space group $P4/nmm$). $CeCu_2Si_2$ [8–11] and $CePd_2Si_2$ [12–15] are two such compounds which form in $ThCr_2Si_2$-type bct structure and present exotic physical properties. Kondo lattice $CeCu_2Si_2$ exhibits magnetic fluctuations driven unconventional heavy fermion superconductivity coexisting with long range antiferromagnetic ordering [8–11]. Kondo lattice heavy fermion $CePd_2Si_2$ exhibits long range antiferromagnetic ordering at ambient pressure, and a pressure induced superconductivity develops (near 28 kbar) upon suppressing the antiferromagnetic order which is accompanied with a non-Fermi liquid behavior [12–15].

In a recent study we investigated the physical properties of a Ce-based 122 compound $CeRh_2Ga_2$ which forms in $CaBe_2Ge_2$-type primitive tetragonal structure (space group $P4/nmm$, No. 129) [16]. The

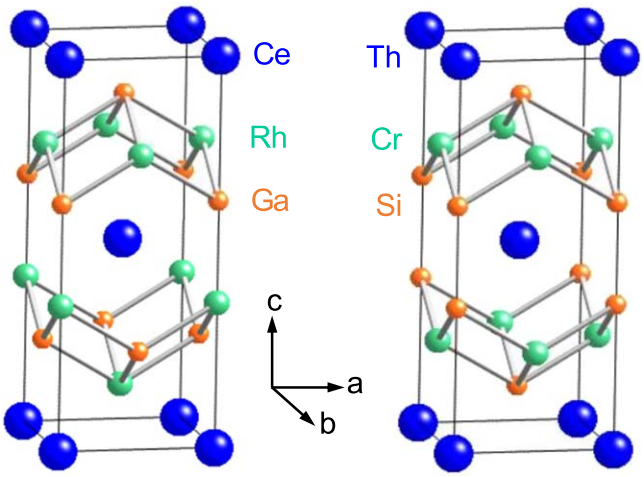

Figure 1. $CaBe_2Ge_2$-type primitive tetragonal structure (space group $P4/nmm$) of $CeRh_2Ga_2$ (left) compared with the $ThCr_2Si_2$-type body centered tetragonal structure (space group $I4/mmm$) (right).

$CaBe_2Ge_2$-type primitive tetragonal structure (space group $P4/nmm$) of $CeRh_2Ga_2$ is shown in figure 1. For a comparison the $ThCr_2Si_2$-type body centered tetragonal structure (space group $I4/mmm$) is also shown. Both the structures are layered, however with different stacking orders of Rh/Cr and Ga/Si layers along the c-axis. Our magnetic susceptibility $\chi(T)$, heat capacity $C_p(T)$ and electrical resistivity $\rho(T)$ measurements on annealed polycrystalline $CeRh_2Ga_2$ revealed a Kondo lattice heavy fermion behavior with a paramagnetic ground state down to 1.85 K [16]. While the overall behavior of resitivity could be described by Kondo effect and crystal electric field effects, the $\rho(T)$ also presents an anomalous increase below 280 K and an unusual upturn below 20 K whose origins are not clear. The low-T upturn in $CeRh_2Ga_2$ is similar to the behavior of ρ of Kondo semimetals $Ce_3Bi_4Pd_3$ [17] and CeNiSn [18].

A parallel study by Nesterenko *et al* [19] also reported an absence of magnetic ordering in $CeRh_2Ga_2$ down to 1.72 K. However, they reported significant atomic disorder on one Rh (2*c*) and one Ga (2*a*) sites for $CaBe_2Ge_2$-type structure of $CeRh_2Ga_2$ [19]. Nesterenko *et al* [19] also collected x-ray diffraction (XRD) data at 173 K, however they did not find any clear evidence for a structural phase transition. They observed two large peaks in the difference Fourier lists of the low temperature XRD of $CeRh_2Ga_2$, located close to the Rh (2*c*) and Ga (2*a*) positions and accordingly refined XRD data by inserting two additional sites, one for Rh (8*i*) and one for Ga (8*i*) (not present in $CaBe_2Ge_2$-type structure) and concluded presence of one Rh and one Ga disordered sites [19]. They also refined the room temperature XRD data with these modifications and suggested for the presence of atomic disorder even at room temperature. In a recent work, Seidel *et al* [20] reported a $CaBe_2Ge_2$-type structure for the nonmagnetic analog $LaRh_2Ga_2$ where they refine XRD data using anharmonic atomic displacement parameters for Rh (2*c*) site. Seidel *et al* [20] also mention presence of complex higher-dimensional structural modulation at room temperature in $CeRh_2Ga_2$ as well as in $PrRh_2Ga_2$.

In a recent theoretical work Chen *et al* [21] suggested that the low temperature state of $CeRh_2Ga_2$ could be a Kondo-driven semimetal phase. Chen *et al* [21] proposed that the strong correlations may cooperate with the crystalline symmetry to develop a gapless topological state. According to them Ce-compounds crystallizing in space group $P4/nmm$ (No 129) provide the key-ingredients for the realization of a Weyl-Kondo semimetal phase. They identified two compounds from space group No. 129, namely $CeRh_2Ga_2$ [16] and $CePt_2Si_2$ [22, 23], both of which remain paramagnetic (down to 1.85 K and 0.06 K, respectively) and have strong electronic correlations, and present semimetal like $\rho(T)$ behavior, to be promising candidates for the realization of Kondo-driven semimetal phase.

Motivated by the fact that one can realize a Weyl-Kondo semimetal phase in $CeRh_2Ga_2$ here we extend our investigations on this compound. In [16] we reported the results on an annealed sample. Here we present the results of $\chi(T)$, $C_p(T)$ and $\rho(T)$ of as-arc-melted sample and compare them with those of the annealed sample, which should be of interest in understanding the physical properties of $CeRh_2Ga_2$. We find that at low temperatures the $\rho(T)$ of as-arc-melted sample significantly differs from that of the annealed sample—while the $\rho(T)$ data of annealed sample presents an upturn (conjectured as a Kondo semimetal feature [21]), the $\rho(T)$ of as-arc-melted sample presents a Fermi-liquid behavior.

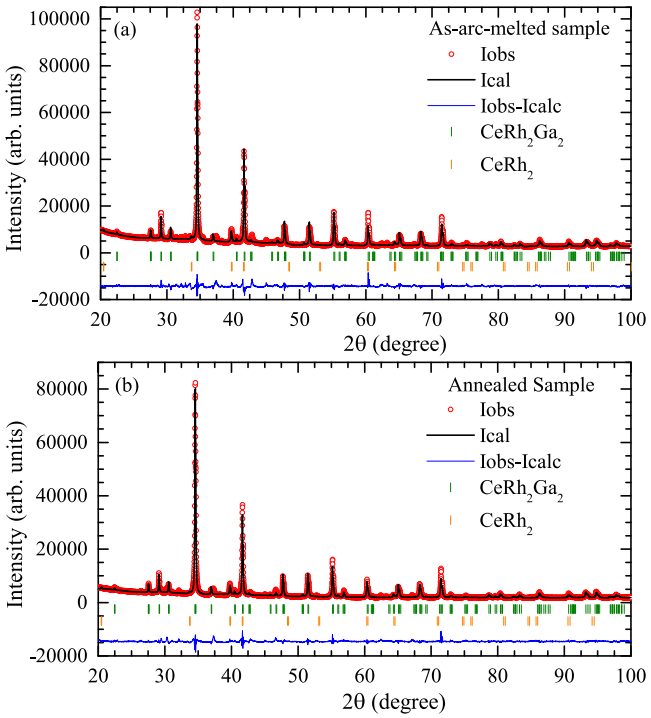

Figure 2. Room temperature powder x-ray diffraction pattern (Cu K_α radiation) of (a) as-arc-melted sample and (b) annealed sample [16] of $CeRh_2Ga_2$ along with the two phase Rietveld refinement profile ($CaBe_2Ge_2$-type tetragonal structure for $CeRh_2Ga_2$). The Rietveld refinement shown by the solid black curves represent major contribution from the bulk $CeRh_2Ga_2$ and a tiny amount of impurity phase $CeRh_2$. The Bragg peak positions for the $CeRh_2Ga_2$ and $CeRh_2$ phases are shown by the short vertical bars. The differences between the experimental and calculated intensities are shown by the lowermost blue curves.

2. Experimental

Polycrystalline samples of $CeRh_2Ga_2$ were prepared by the standard arc melting technique under the inert atmosphere as described in [16]. The high-purity ($\geqslant$99.9%) Ce, Rh and Ga were taken in stoichiometric ratio and arc-melted on a water cooled copper hearth in an Argon atmosphere. During the melting process the samples were flipped and remelted four-five times to achieve a homogeneous sample of $CeRh_2Ga_2$. The sample obtained so we refer as 'as-arc-melted' sample. To improve the sample quality further, part of the as-arc-melted sample was annealed at 800 °C for a period of three weeks which we refer as 'annealed' $CeRh_2Ga_2$. The sample qualities of both as-arc-melted and annealed $CeRh_2Ga_2$ were checked by powder x-ray diffraction. Magnetization M measurements of both as-arc-melted and annealed samples were made using a commercially available superconducting quantum interference device (SQUID) magnetometer (MPMS, Quantum Design Inc.) as a function of both temperature T and magnetic field H. The heat capacity $C_p(T)$ and electrical resistivity $\rho(T)$ and $\rho(H)$ were measured using the heat capacity and resitivity options of a physical properties measurement system (PPMS, Quantum Design Inc.).

3. Results and discussion

Figure 2 shows the powder x-ray diffraction data of both as-arc-melted and annealed $CeRh_2Ga_2$ collected at room temperature. While the bulk of the sample formed in the desired $CeRh_2Ga_2$ phase, the XRD data also show the presence of a small amount of impurities in both as-arc-melted and annealed samples, the impurity fraction being slightly higher in as-arc-melted sample. The Rietveld refinement profiles (see figure 2) of the XRD patterns using FullProf [24] confirmed the $CaBe_2Ge_2$-type primitive tetragonal (space group $P4/nmm$, No. 129) structure of $CeRh_2Ga_2$. The lattice parameters and refined atomic coordinates are listed in table 1. A two-phase refinement, as shown in figure 2, identifies the major impurity phase to be $CeRh_2$ which according to Reitveld refinement is around 3.5% in as-arc-melted sample and 2.9% in annealed sample. Accordingly we estimate about 5% impurities in annealed sample, and that in as-arc-melted sample is estimated to be less than 8% (including unidentified impurities). The impurity phase $CeRh_2$ is paramagnetic in nature and exhibits intermediate valence behavior [25, 26].

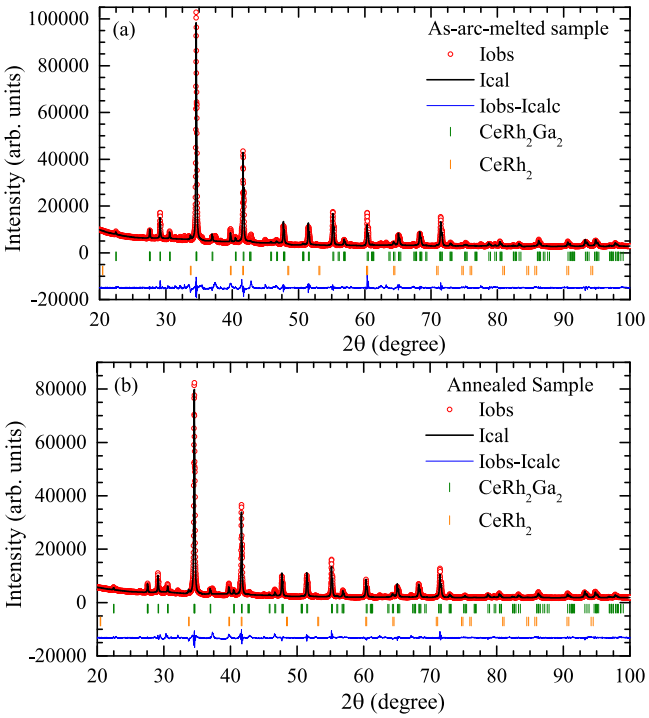

Figure 3. Room temperature powder x-ray diffraction pattern (Cu K_α radiation) of (a) as-arc-melted sample and (b) annealed sample [16] of $CeRh_2Ga_2$ along with the Rietveld refinement profile for modified $CaBe_2Ge_2$-type structure. The Bragg peak positions are shown by the short vertical bars and the differences between the experimental and calculated intensities are shown by the lowermost blue curves.

Table 1. Crystallographic parameters obtained from the Rietveld refinement of the powder XRD data of as-arc-melted and annealed $CeRh_2Ga_2$ with a $CaBe_2Ge_2$-type primitive tetragonal structure (space group $P4/nmm$). The Ce, Rh1, Rh2, Ga1, and Ga2 occupy the Wyckoff positions 2c (1/4, 1/4, z_{Ce}), 2a (3/4, 1/4, 0), 2c (1/4, 1/4, z_{Rh2}), 2b (3/4, 1/4, 1/2) and 2c (1/4, 1/4, z_{Ga2}), respectively. Also listed are the parameters obtained from the analysis of the inverse magnetic susceptibility $\chi^{-1}(T)$ by the modified Curie-Weiss law.

Parameters	As-arc-melted $CeRh_2Ga_2$	Annealed $CeRh_2Ga_2$
Lattice parameters		
a (Å)	4.3331(1)	4.3321(1)
c (Å)	9.7169(2)	9.7202(2)
Atomic coordinates		
z_{Ce}	0.2438(4)	0.2435(3)
z_{Rh2}	0.6142(3)	0.6128(3)
z_{Ga2}	0.8549(6)	0.8527(4)
$\chi^{-1}(T)$ modified CW-fit		
χ_0 (emu/mol)	$8.1(2) \times 10^{-4}$	$6.4(2) \times 10^{-4}$
C (emu K/mole)	0.652(3)	0.778(2)
θ_p (K)	−14.7(5)	−27.6(6)
μ_{eff} (μ_B/Ce)	2.28(1)	2.49(1)

We also tried to refine our XRD data for disordered Rh and Ga sites as suggested by Nesterenko *et al* [19], by inserting Rh (8*i*) and Ga (8*i*), however, we found that if the occupancy of Ga (8*i*) site is allowed to vary freely then it picks a negative value with an occupancy of about 95% at Ga (2*b*) site [Note: in our choice of coordinates Ga atoms occupy 2*c* and 2*b* sites which is different from that in [19] where Ga atoms are allocated to 2*c* and 2*a* sites]. Hence in the final refinement we removed Ga (8*i*) and kept only Rh (8*i*). The refinement profiles with this modified structure for as-arc-melted and annealed samples are presented in figure 3. There is a little

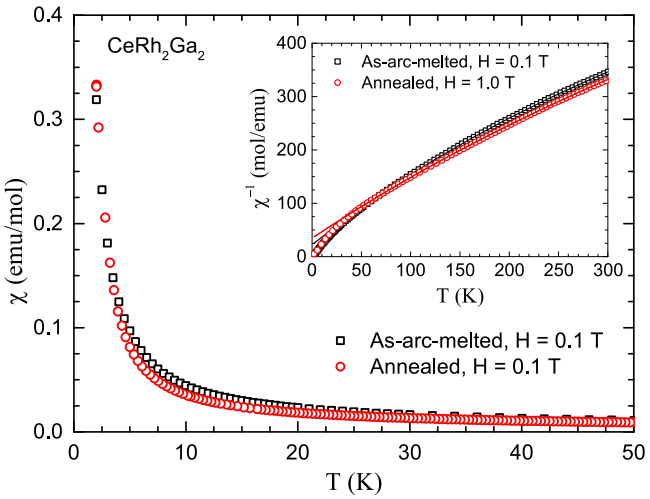

Figure 4. Zero-field-cooled magnetic susceptibility χ of as-arc-melted and annealed $CeRh_2Ga_2$ as a function of temperature T for $2\ K \leqslant T \leqslant 50\ K$ measured in a magnetic field $H = 0.1$ T. Inset: Inverse magnetic susceptibility $\chi^{-1}(T)$ for $2\ K \leqslant T \leqslant 300\ K$.

Table 2. Crystallographic parameters obtained from the Rietveld refinement of the powder XRD data of as-arc-melted and annealed $CeRh_2Ga_2$ with a modified $CaBe_2Ge_2$-type primitive tetragonal structure (space group $P4/nmm$).

Atom	Wyckoff position	x	y (annealed/ as-arc-melted)	z (annealed/ as-arc-melted)	Occupancy (annealed/ as-arc-melted)
Ce	2*c*	1/4	1/4	0.2382(3)/0.2372(7)	1
Rh1	2*a*	3/4	1/4	0	1
Rh2	2*c*	1/4	1/4	0.6166(6)/0.602(7)	0.67(2)/0.45(2)
Rh3	8*i*	1/4	0.106(6)/0.194(9)	0.619(2)/0.642(7)	0.35(2)/0.52(2)
Ga1	2*b*	3/4	1/4	1/2	1
Ga2	2*c*	1/4	1/4	0.8620(5)/0.867(2)	1

improvement in R-factors (e.g. from 4.23 for $CaBe_2Ge_2$-type structure to 3.93 for modified $CaBe_2Ge_2$-type structure for annealed sample). The crystallographic parameters obtained so are listed in table 2. We notice that for the annealed sample Rh (2c) has an occupancy of 67(2)% and the remaining Rh occupy Rh (8*i*) site which refinement yields to be 35(2)%. On the other hand for the as-arc-melted sample these occupancy percentages are 45(2)% and 52(2)%, respectively, reflecting a higher degree of disorder in as-arc-melted sample.

Figure 4 shows the low-temperature ($2\ K \leqslant T \leqslant 50\ K$) zero-field-cooled (ZFC) dc magnetic susceptibility $\chi(T)$ data of as-arc-melted as well as annealed $CeRh_2Ga_2$ measured in an applied magnetic field $H = 0.1$ T. No anomaly related to magnetic phase transition is seen clearly in $\chi(T)$ data down to 2 K. However, a rapid increase and relatively large magnitude of χ at low-T might be an indication of the presence of short-range correlations. The ZFC and field-cooled (FC) $\chi(T)$ do not show any irreversibility (FC data not shown). The $\chi(T)$ data of as-arc-melted and annealed samples show similar behavior. The inverse magnetic susceptibility $\chi^{-1}(T)$ data of both as-arc-melted and annealed samples are shown in the inset of figure 4 over $2\ K \leqslant T \leqslant 300\ K$ measured at 0.1 T and 1.0 T, respectively. The $\chi(T)$ data follow the modified Curie-Weiss (CW) behavior: $\chi(T) = \chi_0 + C/(T - \theta_p)$. A fit of the $\chi^{-1}(T)$ data with the modified CW law over $100\ K \leqslant T \leqslant 300\ K$ yielded paramagnetic Weiss temperature $\theta_p = -14.7(5)$ K and effective moment $\mu_{eff} = \sqrt{8C} = 2.28(1)\mu_B$/Ce for as-arc-melted sample, and $\theta_p = -27.6(6)$ K and $\mu_{eff} = 2.49(1)\mu_B$/Ce for annealed sample. The values of θ_p and μ_{eff} are different for as-arc-melted and annealed samples. While the μ_{eff} of annealed sample is close to the theoretical value of 2.54 μ_B/Ce expected for Ce^{3+} ions ($J = 5/2$), the μ_{eff} of as-arc-melted sample is smaller. The reduced value of μ_{eff} for the as-arc-melted sample could be the result of the Kondo coherence which is very much clear from the electrical resistivity data of the as-arc-melted sample (data presented later). Annealed sample for which there is no reduction in μ_{eff} lacks Kondo coherence in electrical resistivity. The fit parameters χ_0, C and θ_p obtained from the analysis of $\chi^{-1}(T)$ data for both as-arc-melted and annealed $CeRh_2Ga_2$ are listed in table 1.

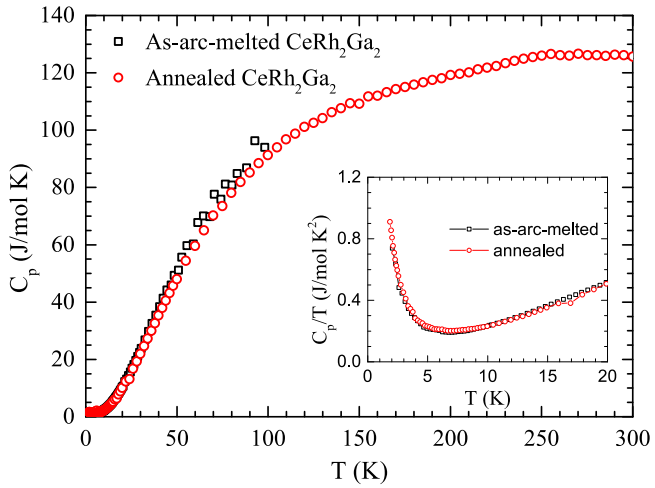

Figure 5. Heat capacity C_p of as-arc-melted and annealed $CeRh_2Ga_2$ samples as a function of temperature T measured in zero field for 1.85 K $\leqslant T \leqslant$ 300 K. Inset: C_p/T versus T plot showing the upturn feature at low-T.

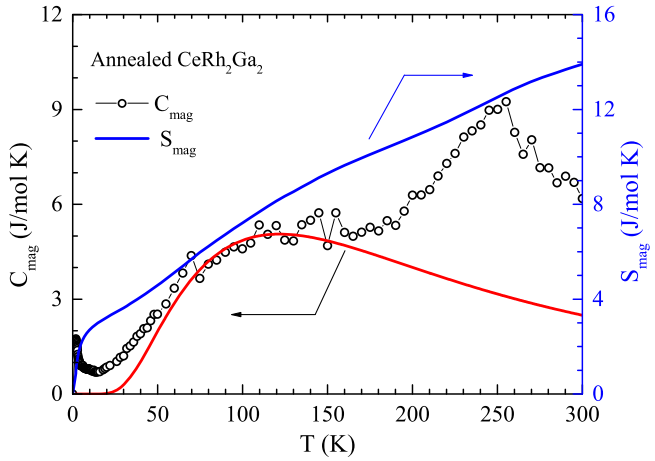

Figure 6. Magnetic contribution to heat capacity C_{mag} and magnetic entropy S_{mag} as a function of temperature T for annealed $CeRh_2Ga_2$ sample. The solid red curve represents the crystal electric field contribution to the heat capacity of $CeRh_2Ga_2$.

Figure 5 shows the heat capacity $C_p(T)$ data of as-arc-melted and annealed $CeRh_2Ga_2$. As can be seen from figure 5, the low-T $C_p(T)$ of as-arc-melted sample is similar to that of the annealed sample, though the $C_p(T)$ data of as-arc-melted sample is little noisy. While the low-T $C_p(T)$ data do not show any clear anomaly related to a magnetic phase transition down to 1.85 K, the high-T $C_p(T)$ data of annealed sample show a weak broad anomaly around 255 K, very likely related to a structural change in view of the corresponding anomaly in electrical resistivity data (discussed below). The 255 K anomaly is very clear in the magnetic contribution to heat capacity $C_{mag}(T)$ (see figure 6) which was obtained by subtracting the phonon contribution using the $C_p(T)$ of isostructural nonmagnetic reference compound $LaRh_2Ga_2$ from the $C_p(T)$ of $CeRh_2Ga_2$. The related compound $CePd_2Ga_2$ (which also forms in $CaBe_2Ge_2$-type primitive tetragonal structure) exhibits a structural transition from tetragonal to triclinic structure near 125 K [27], we suspect a structural change could be the possible origin of an anomaly near 255 K in $CeRh_2Ga_2$ (no structural transition was observed in laboratory based low temperature XRD in [19] though). A similar structural transition has also been observed in $LaPd_2Ga_2$ near 62 K [27]. A comparison of the ratio c/a of $CeRh_2Ga_2$ ($c/a = 2.24$) to that of $CePd_2Ga_2$ ($c/a = 2.22$) does suggest that similar to $CePd_2Ga_2$, $CeRh_2Ga_2$ may also be structurally unstable.

As can be seen from figure 6, apart from the 255 K anomaly, the $C_{mag}(T)$ also exhibits a broad Schottkey type anomaly with a maximum around 150 K which could be associated with the splitting of 6-fold degenerate ground state multiplet of Ce^{3+} ($J = 5/2$). Considering that the six-fold degenerate ground multiplet of Ce^{3+} splits into three doublets under the action of crystal electric field, we analyzed the $C_{mag}(T)$ data by a three-level CEF model. The fitting of the $C_{mag}(T)$ by the CEF model is shown by the solid red curve in the inset of figure 6. Our analysis of $C_{mag}(T)$ of $CeRh_2Ga_2$ suggests the splitting between the ground state doublet and the first excited

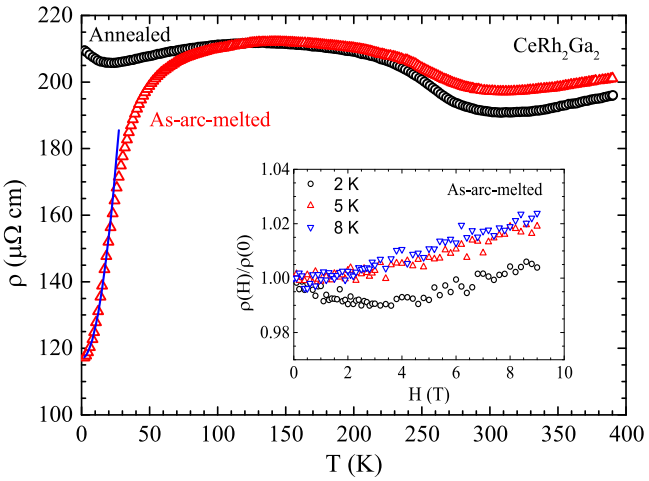

Figure 7. Electrical resistivity ρ of as-arc-melted and annealed $CeRh_2Ga_2$ samples as a function of temperature T for 2 K $\leqslant T \leqslant$ 390 K measured in zero magnetic field. The solid red curve is a fit of $\rho(T)$ data by $\rho(T) = \rho_0 + AT^2$ in 2 K $\leqslant T \leqslant$ 20 K. Inset: ρ of as-arc-melted sample as a function of applied magnetic field H for $0 \leqslant H \leqslant 9$ T, normalized as $\rho(H)/\rho(0)$ for the indicated temperatures.

doublet to be 220 K, and that between the ground state and the second excited doublet to be 480 K. More details about the CEF-model fitting of $C_{mag}(T)$ data can be found in [28–31]. Because of the presence of Kondo effect and 255 K structural anomaly the CEF splitting energies estimated this way are only the rough estimates. An inelastic neutron scattering measurement is desired for a better estimate of CEF level scheme. The magnetic entropy $S_{mag}(T)$ estimated from the $C_{mag}(T)$ data, as shown in the inset of figure 5, attains a value of 13.9 J/mol K^2 at 300 K, which is about 93% of R ln 6.

The low-T $C_p(T)$ of annealed $CeRh_2Ga_2$ sample shows an upturn below 5 K (see inset of figure 5). This upturn feature is also seen in the low-T $C_p(T)$ of as-arc-melted sample (inset of figure 5). This upturn feature of $C_p(T)$ and a corresponding rapid increase in χ may be a manifestation of a magnetic phase transition at T lower than 2 K.

Figure 7 shows the $\rho(T)$ data of $CeRh_2Ga_2$ measured on both as-arc-melted and annealed samples for 2 K $\leqslant T \leqslant$ 390 K. A Kondo lattice behavior can be inferred from the T dependence of ρ. As can be seen from figure 7, the $\rho(T)$ of as-arc-melted and annealed samples show marked difference at low-T. The $\rho(T)$ of as-arc-melted sample shows a sharp decrease below 50 K (with a residual resistivity of $\approx$118 $\mu\Omega$ cm at 2 K) which could be understood to be the result of Kondo coherence. On the other hand, the $\rho(T)$ of annealed sample shows a minima near 20 K and lacks Kondo coherence. Further, it is seen that the $\rho(T)$ of both as-arc-melted and annealed samples show anomalous increase below 280 K. This anomalous increase cannot be accounted by Kondo scattering alone and could be due to a manifestation of possible structural change. The resistivity upturn below 280 K is consistent with the heat capacity anomaly near 255 K.

At $T < 20$ K, the $\rho(T)$ of annealed $CeRh_2Ga_2$ sample shows a weak increase with decreasing T. This upturn in low-T resistivity of the annealed sample is similar to those of the Kondo semimetals $Ce_3Bi_4Pd_3$ [17] and CeNiSn [18]. Theoretically, the development of the Weyl-Kondo semimetal behavior requires the breakdown of either time-reversal symmetry or inversion symmetry (or both). With a *P4/nmm* space group the crystal structure of $CeRh_2Ga_2$ lacks a mirror symmetry along c-axis (local inversion symmetry breaking) and hence fulfills the key requirement for the development of Weyl fermions. Further, as evidenced by the moderately enhanced Sommerfeld coefficient, $CeRh_2Ga_2$ also has strong electronic correlations. According to Chen *et al* [21] the synergy between the strong correlation and the crystal symmetry may provide a favorable condition for the development of a gapless topological state in $CeRh_2Ga_2$. However, this aspect needs further investigations, preferably on the single crystal $CeRh_2Ga_2$.

On the other hand, with a T^2 temperature dependence, the low-T $\rho(T)$ data of as-arc-melted $CeRh_2Ga_2$ sample indicates a Fermi liquid behavior. The reproducibility of Fermi liquid-like behavior in as-arc-melted sample has been checked by measuring the resistivity of two different batches of as-arc-melted samples, both present qualitatively similar overall features of Kondo effect, structural transition-like anomaly and Fermi liquid-like behavior. The observation of T^2 dependence at low-T in the case of the as-arc-melted sample is consistent with the disorder-driven Fermi-liquid feature. Apparently our as-arc-melted sample possesses higher defects and inhomogeneities which is minimized upon annealing and hence annealed $CeRh_2Ga_2$ sample lacks the Fermi-liquid feature. The presence of higher defects and inhomogeneities has been suggested to relax the

constraint to the lattice momentum conservation which in turn enlarges the phase space for various scattering channels to establish a T^2 dependence [32]. Another possible origin of the difference in the T-dependence of low-T $\rho(T)$ of as-arc-melted and annealed samples could be due to a change in the coherence of the structural modulation, which however needs to be verified by techniques like high-resolution synchrotron-XRD.

A fit of $\rho(T)$ data by $\rho(T) = \rho_0 + AT^2$ is shown by the solid blue curve in figure 7. The fit of $\rho(T)$ over 2 K $\leqslant T \leqslant$ 20 K gives $\rho_0 = 117.0(2)$ $\mu\Omega$ cm and $A = 9.18(9) \times 10^{-2}$ $\mu\Omega$ cm/K^2. With $\gamma \approx 130$ mJ/mol K^2 [16], the Kadowaki-Woods ratio $R_{KW} = A/\gamma^2$ is found to be 0.54×10^{-5} $\mu\Omega$ cm/(mJ/mol K)^2 which is of similar order as typically observed in strongly correlated and heavy fermion systems, the universal value of R_{KW} being 1×10^{-5} $\mu\Omega$ cm/(mJ/mol K)^2 [33].

We also measured the H dependence of ρ of the as-arc-melted sample of $CeRh_2Ga_2$ at selected temperatures 2 K, 5 K and 8 K. The $\rho(H)$ data are presented in the inset of figure 7, normalized as $\rho(H)/\rho(0)$, where $\rho(H)$ refers to the value of ρ measured with H applied and and $\rho(0)$ to that without H at a given temperature. The ρ shows only a weak H dependence. It is seen that at 2 K initially ρ decreases with increasing H up to about 3.0 T, above which ρ starts increasing again. At 5 K and 8 K the ρ increases with H almost over the entire range of H, with a magnetoresistance of about 2% at 9 T. An increase in ρ with increasing H could be understood to be the result of classical Lorentzian modification of the trajectory of charge carriers in the magnetic field. The $\rho(H)$ behavior at 2 K can be understood to comprise of an additional negative component on account of parallel alignment of spins along the applied field associated with the presence of short range correlations that dominates at fields lower than 3.0 T whereas positive contribution due to Lorentzian force dominates at higher fields.

4. Conclusions

We have investigated the effect of annealing on the physical properties of Kondo lattice system $CeRh_2Ga_2$. With a $CaBe_2Ge_2$-type primitive tetragonal structure (space group $P4/nmm$) $CeRh_2Ga_2$ presents a moderate heavy fermion behavior and remains paramagnetic down to 1.85 K. The effect of annealing has been examined by powder XRD, $\chi(T)$, $C_p(T)$ and $\rho(T)$ measurements on the as-arc-melted and annealed $CeRh_2Ga_2$ samples. The XRD data of both as-arc-melted and annealed samples are similar, however the impurity content is little higher (by a few %) in as-arc-melted sample. The T dependences of χ are also similar for both as-arc-melted and annealed samples. The high-T $\chi(T)$ of both the samples follow the modified CW behavior, however they yield a little different values of θ_p and μ_{eff}. The low-T C_p data also look similar for as-arc-melted and annealed samples, they both reveal an upturn in C_p below 5 K very likely associated with a magnetic phase transition at lower temperature. The effect of annealing is quite pronounced in $\rho(T)$. While the high-T $\rho(T)$ of both the samples show similar behavior (apart from the difference in the magnitude of ρ), the low-T $\rho(T)$ data differ significantly. The high-T $\rho(T)$ of both as-arc-melted and annealed samples show an anomalous increase below 280 K. The low-T $\rho(T)$ of as-arc-melted sample presents Kondo coherence and T^2 temperature dependence, and hence a Fermi-liquid behavior. On the other hand, in the case of annealed sample the Kondo coherence is absent and a weak incoherent Kondo scattering leads to an upturn in low-T $\rho(T)$ (at $T < 20$ K) which has been conjectured to be a signature of Kondo-driven semimetal phase [21]. The difference in low-T behavior of $\rho(T)$ of as-arc-melted and annealed samples could be due to the disorder effect or due to a change in the coherence of the structural modulation. Further investigations are required to understand the origin of Fermi-liquid behavior and ascertain whether the upturn below 20 K results due to the opening of an energy gap/hybridization gap or due to a gapless topological state.

Acknowledgments

V K A and D T A acknowledge financial assistance from CMPC-STFC grant number CMPC-09108. D.T.A. would like to thank the Royal Society of London for the Newton Advanced fellowship funding between UK and China, and the International Exchange funding between UK and Japan. DTA also thanks EPSRC UK (Grant No. EP/W00562X/1) for funding. A.B. would like to acknowledge DST, India (SR/NM/Z-07/2015) for the financial support and JNCASR for managing the project, and SERB for CRG Grants (CRG/2020/000698 & CRG/2022/008528) and UGC-DAE-CRS grant (CRS/2021-22/03/549).

Data availability statement

All data that support the findings of this study are included within the article (and any supplementary files).

ORCID iDs

V K Anand https://orcid.org/0000-0003-2023-7040
D T Adroja https://orcid.org/0000-0003-2280-079X

References

[1] Stewart G R 1984 Heavy-fermion systems *Rev. Mod. Phys.* **56** 755
[2] Stewart G R 2001 Non-Fermi-liquid behavior in d- and f-electron metals *Rev. Mod. Phys.* **73** 797
[3] Amato A 1997 Heavy-fermion systems studied by μSR technique *Rev. Mod. Phys.* **69** 1119
[4] Riseborough P S 2000 Heavy fermion semiconductors *Adv. Phys.* **49** 257
[5] Löhneysen H V, Rosch A, Vojta M and Woelfle P 2007 Fermi-liquid instabilities at magnetic quantum phase transitions *Rev. Mod. Phys.* **79** 1015
[6] Pfleiderer C 2009 Superconducting phases of f-electron compounds *Rev. Mod. Phys.* **81** 1551
[7] Si Q and Steglich F 2010 Heavy fermions and quantum phase transitions *Science* **329** 1161
[8] Steglich F, Aarts J, Bredl C D, Licke W, Meschede D, Franz W and Schäfer H 1979 Superconductivity in the presence of strong pauli paramagnetism: $CeCu_2Si_2$ *Phys. Rev. Lett.* **43** 1892
[9] Steglich F *et al* 1996 New observations concerning magnetism and superconductivity in heavy-fermion metals *Physica* B **223-224** 1
[10] Stockert O *et al* 2011 Magnetically driven superconductivity in $CeCu_2Si_2$ *Nat. Phys.* **7** 119
[11] Kittaka S, Aoki Y, Shimura Y, Sakakibara T, Seiro S, Geibel C, Steglich F, Ikeda H and Machida K 2014 Multiband superconductivity with unexpected deficiency of nodal quasiparticles in $CeCu_2Si_2$ *Phys. Rev. Lett.* **112** 067002
[12] Grier B H, Lawrence J M, Murgai V and Parks R D 1984 Magnetic ordering in CeM_2Si_2 (M=Ag, Au, Pd, Rh) compounds as studied by neutron diffraction *Phys. Rev.* B **29** 2664
[13] Van Dijk N H, Fåk B, Charvolin T, Lejay P and Mignot J M 2000 Magnetic excitations in heavy-fermion $CePd_2Si_2$ *Phys. Rev.*B **61** 8922
[14] Grosche F M, Walker I R, Julian S R, Mathur N D, Freye D M, Steiner M J and Lonzarich G G 2001 Superconductivity on the threshold of magnetism in $CePd_2Si_2$ and $CeIn_3$ *J. Phys.: Condens. Matter* **13** 2845
[15] Demuer A, Jaccard D, Sheikin I, Raymond S, Salce B, Thomasson J, Braithwaite D and Flouquet J 2001 Further pressure studies around the magnetic instability of $CePd_2Si_2$ *J. Phys.: Condens. Matter* **13** 9335
[16] Anand V K, Adroja D T, Bhattacharyya A, Klemke B and Lake B 2017 Kondo lattice heavy fermion behavior in $CeRh_2Ga_2$ *J. Phys.: Condens. Matter* **29** 135601
[17] Dzsaber S, Prochaska L, Sidorenko A, Eguchi G, Svagera R, Waas M, Prokofiev A, Si Q and Paschen S 2017 Kondo insulator to semimetal transformation tuned by spin-orbit coupling *Phys. Rev. Lett.* **118** 246601
[18] Nakamoto G, Takabatake T, Fujii H, Minami A, Maezawa K, Oguro I and Menovsky A A 1995 Crystal growth and characterization of the kondo semimetal CeNiSn *J. Phys. Soc. Jpn.* **64** 4834
[19] Nesterenko S, Avzuragova V, Tursina A and Kaczorowski D 2017 Structural peculiarities and magnetic properties of a novel cerium gallide $CeRh_2Ga_2$ *J. Alloys Comp.* **717** 136
[20] Seidel S, Schubert L, Hoffmann R-D and Pöttgen R 2020 Centrosymmetric $LaRh_2Ga_2$ *Z. Kristallogr.* **235** 41
[21] Chen L *et al* 2022 Topological semimetal driven by strong correlations and crystalline symmetry *Nature Phys.* **18** 1341
[22] Gignoux D, Schmitt D, Zerguine M, Ayache C and Bonjour E 1986 Magnetic properties of a new Kondo lattice compound: $CePt_2Si_2$ *Phys. Lett.* A **117** 145
[23] De Réotier P D, Yaouanc A, Calemczuk R, Huxley A D, Marcenat C, Bonville P, Lejay P, Gubbens P C M and Mulders A M 1997 $CePt_2Si_2$: A Kondo lattice compound with no magnetic ordering down to 0.06 K *Phys. Rev.*B **55** 2737
[24] Rodríguez-Carvajal J 1993 Recent advances in magnetic structure determination by neutron powder diffraction *Physica* B **192** 55 Program Fullprof, LLB-JRC, Laboratoire Léon Brillouin, CEA-Saclay, France
[25] Barberis G E, Roden B, Weidner P, Gupta L C, Davidov D and Felner I 1982 Intermediate valence effects in the magnetic behaviour of $Ce(Rh_xPt_{1-x})_2$ laves phase compounds *Solid State Commun.* **42** 659
[26] Sugawara H *et al* 1994 Single crystal growth and electrical properties of $CeRh_2$ and $CeIr_2$ *J. Phys. Soc. Jpn.* **63** 1502
[27] Kitagawa J and Ishikawa M 1999 Magnetic properties and structural phase transition of $CePd_2Ga_2$ with $CaBe_2Ge_2$-type structure *J. Phys. Soc. Jpn.* **68** 2380
[28] Anand V K, Adroja D T, Britz D, Strydom A M, Taylor J W and Kockelmann W 2016 Crystal-field states of kondo lattice heavy fermions $CeRuSn_3$ and $CeRhSn_3$ *Phys. Rev.* B **94** 014440
[29] Anand V K, Adroja D T and Hillier A D 2013 Magnetic and transport properties of $PrRhSi_3$ *J. Phys.: Condens. Matter* **25** 196003
[30] Prasad A, Anand V K, Paramanik U B, Hossain Z, Sarkar R, Oeschler N, Baenitz M and Geibel C 2012 Ferromagnetic ordering in $CeIr_2B_2$: Transport, magnetization, specific heat and NMR studies *Phys. Rev.*B **86** 014414
[31] Layek S, Anand V K and Hossain Z 2009 Valence fluctuation in $Ce_2Co_3Ge_5$ and crystal field effect in Pr2Co3Ge5 *J. Magn. Magn. Mater.* **321** 3447
[32] ElMassalami M and Neto M B Silva 2021 Superconductivity, Fermi-liquid transport, and universal kinematic scaling relation for metallic thin films with stabilized defect complexes *Phys. Rev.*B **104** 014520
[33] Kadowaki K and Woods S B 1986 Universal relationship of the resistivity and specific heat in heavy-Fermion compounds *Solid State Commun.* **58** 507